



0021-8502 (94) 00092-1

## ASPIRATION EFFICIENCY OF A THIN-WALLED CYLINDRICAL PROBE REAR-FACING THE WIND

X. Wen and D. B. Ingham

Department of Applied Mathematical Studies, University of Leeds, Leeds LS2 9JT, U.K.

*(First received 3 January 1994; and in final form 30 May 1994)*

**Abstract**—The sampling mechanism of a thin-walled, cylindrical aerosol sampling probe which faces directly away from the wind ( $180^\circ$  orientation) is numerically investigated. The turbulent fluid flow is predicted by employing the control volume, finite-difference method and the  $k-\epsilon$  turbulence model. The particle trajectories are calculated by integrating the particle equations of motion and thus the aspiration efficiency of the sampler is determined. The numerical results have been obtained for two very long thin-walled cylindrical samplers of diameters  $D = 2$  and  $5$  cm which have zero thickness and the operating conditions as used in the experimental investigations of Vincent *et al.* (1986, *J. Aerosol Sci.* 17, 211–224) have been considered. The dependence of the characteristics of the fluid flow and the aspiration efficiency on the freestream air speed, the diameter of the sampler and the ratio of the freestream speed to the sampling speed, have been thoroughly investigated. It is concluded that the numerical results for the aspiration efficiency are in reasonable agreement with all the existing experimental data for thin-walled samplers which are placed at  $180^\circ$  to the direction of the wind.

### INTRODUCTION

Aerosol samplers are widely used in the sampling of aerosols in industrial hygiene in order to determine the concentration of particles in relevant size fractions in the ambient atmosphere and in clean rooms. In aerosol sampling numerous methods and devices have been developed and a large number of experimental and theoretical investigations have been performed. An important aspect of the sampling process is to determine the aspiration efficiency of a sampler and this is defined as the ratio of the particle concentration in the air sampled to the particle concentration far from the sampling location. The presence of the sampler inevitably disturbs the movement of the air and causes a distortion of the air flow. This distortion not only changes the motion of the original ambient atmosphere but also affects the motion of the particles and this may result in significant changes in the particle distribution in the vicinity of the sampler.

Thin-walled sampling probes are used primarily for duct sampling (isokinetic) when the air velocity is known and the early experimental work and theoretical analysis concentrated on the situation when the sampler faces the wind, see for example Badzioch (1959), Vitols (1966), Sehmel (1967), Ruping (1968), Belyaev and Levin (1974), Jayasekera and Davies (1980) and Okazaki *et al.* (1987). These investigations have shown that the aspiration efficiency of the thin-walled sampler is a function of the particle inertia, namely the particle Stokes number,  $St$ , and the ratio,  $R$ , of the undisturbed freestream fluid speed,  $U_0$ , to the sampling speed,  $U_s$ . In this case the air flow appears to take on a relatively simple flow pattern where the flow distortion in front of the sampler is divergent or convergent depending on whether the speed ratio  $R$  is greater or less than unity. Based on the experimental observations of the air flow and the motion of the particles, the early theoretical analyses on this sampler are almost entirely empirical.

In practical applications of thin-walled samplers the operating conditions are much more complicated when the probe is oriented at any angle with respect to the wind. As this angle increases from  $0^\circ$  to an angle of less than  $90^\circ$  the air flow undergoes an increasing distortion when approaching the orifice of the sampler, thus increasing the effective bluntness of the sampler. Recently, some experimental work and semi-empirical analyses have been performed by Durham and Lundgren (1980), Davies and Subari (1982), Vincent *et al.* (1986),

Hangal and Willeke (1990) and Grinshpun *et al.* (1993). These works are based on the general knowledge of the shape of the flow pattern in the vicinity of the sampler and they have proved to give a fairly good understanding of this problem. However, the sampling mechanism is still to be fully revealed. For potential flow past thin-walled samplers at orientations with respect to the flow direction from 0 to 90° a numerical investigation was performed by Dunnett (1990) using the boundary element method. However, this numerical model cannot be extended to situations where this angle of inclination is larger than 90° because the turbulent characteristics of the air flow now play an important role when predicting the aspiration efficiency. When the angle of inclination of the sampler is larger than 90° the air flow is much more complex and the flow pattern no longer appears as simply diverging or converging. Therefore all the previous mathematical models and semi-empirical formulae cannot reveal the principal mechanisms of the sampling process.

Up to now, when the thin-walled sampler is at an angle of inclination larger than 90° there exists only the experimental investigation performed by Vincent *et al.* (1986) and this was for an angle of inclination of 180°. In this paper a qualitative analysis of the experimental data is also presented. The recent paper by Tsai and Vincent (1993) was an impaction model for blunt samplers at angles of 90° and 180°. In the thin-walled cylindrical sampler limit a semi-empirical formula for the aspiration efficiency has been suggested in which the coefficients in the formula were found using a non-linear regression technique. In this work they have only considered, in general, the effects of the bluntness and the air flow pattern in the vicinity of the sampler on the aspiration efficiency. However, when the angle of inclination is greater than 90°, the air entering the sampler is substantially affected by the geometry of the sampler. When the sampler is facing directly backwards to the direction of the oncoming wind then the bluntness of the sampler causes the flow to diverge around the leading edge of the bluff body and near to the wall of the sampler there is a boundary layer. Thus a portion of the air which is sampled will flow into the boundary layer along the external wall of the sampler and finally into the orifice of the sampler. When the diameter of the sampler is small, or the freestream velocity is not large, then a large portion, or even all, of the sampled air will come from the flow in the boundary layer. Because the characteristics of the air flow in the boundary layer are significantly affected by the geometry of the external wall of the sampler, it can be concluded that the influence of the geometry of the sampler cannot be ignored in the sampling process. As sampling is taking place behind the sampler then particles in the vicinity of the orifice which are sampled have to change the direction in which they are moving very rapidly. However, the inertia of a particle in this region may cause the particle to escape and to continue its motion downstream of the sampler. The complicated nature of the air flow around the sampler makes the sampling process quite different from the situation when the sampler is inclined at less than 90° to the wind.

In this paper we consider a thin-walled, cylindrical sampler which faces directly backwards to the oncoming turbulent wind. We have found that when the length of the sampling tube,  $L$ , is much larger than the diameter of the sampler,  $D$  (say  $L/D > 15.0$ ), there exists a fully developed turbulent boundary-layer in the mid-section of the external surface of the sampler and in this vicinity the streamlines are parallel to the walls. Therefore as a first step with such a complicated air flow we investigate a relatively simple case in which the sampling probe is very long, see Fig. 1, and therefore the effect of the bluntness of the upstream surface on the downstream facing sampler has been ignored. The resulting air and flow of particles which we obtain provides some fresh insight into the physics of the sampling process. Of course, the bluntness of the sampler is an important factor in the sampling process, as is the geometry of the sampling probe, and these effects will be included in a future investigation.

When the probe is sufficiently long the turbulent boundary-layer along the external wall of the probe is fully developed at some distance upstream of the orifice of the sampler and we will assume that at the station AA', see Fig. 1, the flow is fully developed. Further, inside and outside of the turbulent boundary-layer on the sampler the particles have had sufficient time to reach the same velocity as that of the air. A full numerical investigation of the

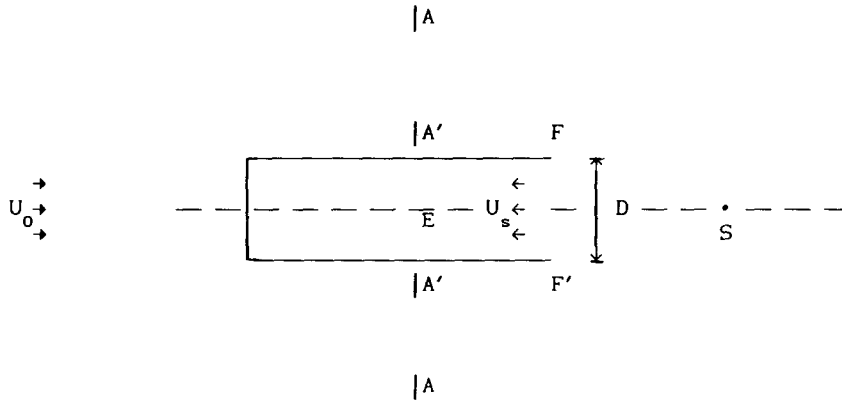


Fig. 1. Schematic diagram of a thin-walled, cylindrical sampler facing directly backwards to the oncoming wind.

turbulent flow has been performed in order to simulate the turbulent air flow by using the turbulent  $k-\epsilon$  model. Once the air flow has been determined then the particle paths have been traced by solving the particle equations of motion from which the aspiration efficiency of the sampler may be obtained.

MATHEMATICAL MODEL

We only consider the domain downstream of the location AA', see Fig. 1, and since the sampler is axisymmetrical we need only consider the solution in the semi-infinite domain ABCSOEA'FA'A as shown in Fig. 2. Cylindrical coordinates are used in which  $r$  is the coordinate in the radial direction and  $z$  is aligned with the axis of symmetry of the sampler and is measured positively in the direction of the freestream. At the location AA' the turbulent flow outside the boundary layer of the probe is fully developed with an average speed  $U_0$ . Within the sampling probe at the location A'E the flow is fully developed turbulent flow in a cylindrical pipe with an average sampling velocity  $U_s$ . Thus we define the velocity ratio  $R = U_0/U_s$ , and assume that the sampling probe has a diameter  $D$  and zero thickness. Because some of the fluid in the region A'A will enter the sampler and some will not, there will be a dividing stream surface which separates these fluids. In particular there will be a point on the axis of symmetry where there is a stagnation point, say the point S, see Fig. 2, and the distance from the stagnation point S to the orifice of the sampling probe is assumed to be  $x_s$ .

We assume that the air flow is turbulent, according to the experimental operating conditions of Vincent *et al.* (1986). In order to simulate the turbulent flow, the standard  $k-\epsilon$  model, see for example Launder and Spalding (1974), has been employed. Therefore the

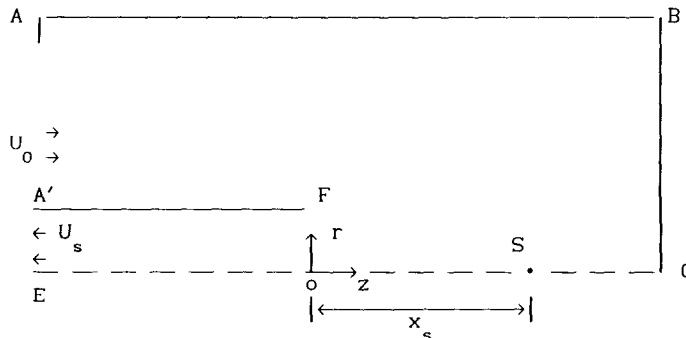


Fig. 2. Computational domain and coordinate system.

momentum equation for the turbulent fluid flow, in vector notation, is given by

$$\mathbf{V} \cdot \nabla \mathbf{V} = -\frac{1}{\rho} \nabla p + \nabla \cdot (v_e \nabla \mathbf{V}) \quad (1)$$

and for incompressible turbulent flow we also have the continuity equation

$$\nabla \cdot \mathbf{V} = 0, \quad (2)$$

where  $\mathbf{V} = u\mathbf{e}_r + w\mathbf{e}_z$ ,  $u$  and  $w$  are the mean values of the turbulent components of the fluid velocity in the radial and axial directions, respectively, and  $\mathbf{e}_r$  and  $\mathbf{e}_z$  are unit vectors in the radial and axial directions, respectively,  $\rho$  is the density of the fluid and  $v_e$  is the effective kinematic viscosity of the fluid and consists of the sum of the laminar kinematic viscosity  $\nu$  and the turbulent kinematic viscosity  $\nu_t$ , i.e.  $v_e = \nu + \nu_t$ .

The governing equations for the turbulent kinetic energy,  $k$ , and the turbulent energy dissipation,  $\varepsilon$ , are

$$(\mathbf{V} \cdot \nabla)k = \nabla \cdot \left[ \left( \nu + \frac{\nu_t}{\sigma_k} \right) \nabla k \right] + \phi - \varepsilon, \quad (3)$$

$$(\mathbf{V} \cdot \nabla)\varepsilon = \nabla \cdot \left[ \left( \nu + \frac{\nu_t}{\sigma_\varepsilon} \right) \nabla \varepsilon \right] + C_1 \frac{\varepsilon}{k} \phi - C_2 \frac{\varepsilon^2}{k}, \quad (4)$$

respectively, where  $\phi$  is the generation of the turbulent energy which is caused by turbulent stresses. The turbulent viscosity is given by

$$\nu_t = C_\mu \frac{k^2}{\varepsilon} \quad (5)$$

and the coefficients which occur in equations (3)–(5) are those employed in similar turbulent flow problems, namely

$$C_\mu = 0.09, \quad \sigma_k = 1.0, \quad \sigma_\varepsilon = 1.3, \quad C_1 = 1.44, \quad C_2 = 1.92.$$

Equations (1)–(5) have to be solved subject to the following boundary conditions:

At the upstream boundary AA':

The radial velocity is such that  $u = 0$ , the axial velocity,  $w$ , satisfies the condition of fully developed turbulent flow, namely  $\partial w / \partial z = 0$ , and the average value of the  $w$  component of velocity is  $U_0$ . The turbulent kinetic energy,  $k$ , and the turbulent dissipation,  $\varepsilon$ , satisfy the conditions  $\partial k / \partial z = 0$  and  $\partial \varepsilon / \partial z = 0$ .

At the freestream boundary AB:

$\partial u / \partial r = 0$  and  $\partial w / \partial r = 0$ , and  $k = (IU_0)^2$ , where  $I$  is the turbulent intensity which is specified by the experimental data of Vincent *et al.* (1986), and the value of  $\varepsilon$  is also specified by the turbulent length scale  $L$  through the experimental data of Vincent *et al.*, namely  $I = 0.06$  and  $L = 7$  cm, and hence the value of  $\varepsilon$  is determined from  $\varepsilon = k^{1.5}/L$ .

At the downstream boundary BC:

$$\frac{\partial u}{\partial z} = 0, \quad \frac{\partial w}{\partial z} = 0, \quad \frac{\partial k}{\partial z} = 0, \quad \frac{\partial \varepsilon}{\partial z} = 0.$$

On the axis of symmetry EC:

$$u = 0, \quad \frac{\partial w}{\partial r} = 0, \quad \frac{\partial k}{\partial r} = 0, \quad \frac{\partial \varepsilon}{\partial r} = 0.$$

At the exit of the sampling probe A'E:

$$\frac{\partial u}{\partial z} = 0, \quad \frac{\partial w}{\partial z} = 0, \quad \frac{\partial k}{\partial z} = 0, \quad \frac{\partial \varepsilon}{\partial z} = 0,$$

and the average axial component of velocity,  $w$ , is  $U_s$ .

On the wall of the sampling probe A'F:

$$u = 0, \quad w = 0, \quad \frac{\partial k}{\partial r} = 0,$$

and the value of  $\varepsilon$  is given by the wall function method.

The control volume, finite-difference method, as described by Ingham and Wen (1993), with a non-staggered grid and the SIMPLEC algorithm, see Patankar (1980) and Van Doormaal and Raithby (1984), has been used to solve equations (1)–(5). In order to guarantee and accelerate the rate convergence of the iterative procedure, the average pressure correction technique developed by Wen and Ingham (1993) was used at the orifice of the sampler. Several non-uniform grid systems were tested for the solution domain with  $-7.1 < z/(D/2) < 7.1$  and  $0 < r/(D/2) < 9.1$ . It was found that when the mesh is finer than a  $90 \times 45$  grid, independent solutions can be produced. In this paper all the results presented were obtained by using a  $110 \times 52$  mesh and approximately 800 iterations can produce accurate results. The computations were performed on a Silicon Graphics Iris Indigo R3000 and typical CPU times were  $O(10^3)$ s.

If the particle Reynolds number is much less than unity the  $i$  component of the Lagrangian equation of motion of the particle takes the form

$$\frac{dx_i}{dt^*} = u_{pi}, \quad (6)$$

$$St \frac{du_{pi}}{dt^*} = \bar{u}_i + u'_i - u_{pi}, \quad (7)$$

where  $St = \gamma^* d_{ae} U_0 / (18\mu D/2)$  is the Stokes number,  $\gamma^*$  is the density of water,  $d_{ae}$  is the particle aerodynamic diameter,  $\mu$  is the viscosity of the air,  $x_i$  is the position of the particle,  $t^* = tU_0/D$  is the non-dimensional time,  $u_{pi}$  is the  $i$  component of the velocity of the particle,  $\bar{u}_i$  is the mean velocity of the fluid and  $u'_i$  is the fluctuating component of the fluid velocity.

Because particles respond to the turbulent motion of the fluid they do not follow the mean motion of the fluid, resulting in particle turbulent diffusion. When the Stokes number of the particle is very small, i.e.  $St \ll 1.0$ , the particle responds to the turbulent fluctuation very rapidly and the particle diffusion is similar to that of the fluid. As the Stokes number increases, the particle diffusion decreases because of the inertia of the particle, and when  $St \gg 1.0$ , the effect of the turbulent motion of the fluid on the motion of the particle becomes negligible. In general there are two models for investigating such particle motions, namely stochastic and non-stochastic. The stochastic model attempts to produce a particle distribution in the fluid by the use of a diffusion coefficient. Peskin (1962) has obtained an estimation of the diffusion coefficient for a one-dimensional flow; but for complex fluid flows, such as the one considered in this paper, no experimental or theoretical work has been performed which gives a reliable estimation for the diffusion coefficient. The stochastic model, see for example Shuen *et al.* (1983), assumes that a particle interacts with a series of turbulent eddies and the fluid velocity fluctuations are isotropic with a Gaussian distribution. By solving equations (6) and (7), the trajectories of many such particles may be calculated and the statistical properties calculated from an ensemble average of such particle motions. This method is much more expensive in computing time than the stochastic model and also the choice of a length scale for the turbulent eddy, the lifetime and the standard deviation of the Gaussian distribution will affect the results obtained using this method.

Generally the turbulent fluctuating velocity is much smaller than the mean fluid velocity and under the assumption of local isotropic turbulence a particle has an equal chance of diffusing in the two directions which are normal to the mean particle motion. Therefore, when there exists a uniform inlet concentration of particles it is expected that the inertia of the particle will be more important than the particle diffusion in the determination of the aspiration efficiency. Therefore, as a first approximation, we neglect the effect of particle

diffusion on the aspiration efficiency of the sampler and this allows us to simplify equation (7) to

$$\text{St} \frac{du_{pi}}{dt^*} = \bar{u}_i - u_{pi}. \quad (8)$$

It is possible that the small discrepancies that occur between the experimental data and the results obtained in this paper may be due to neglecting particle diffusion, the effect of particle inertia on the particles' ability to respond to the turbulent motions of the air. Further work on this aspect is at present being performed.

It has been assumed that at the location AA' the particle has the same velocity as that of the air and that the concentration of particles is constant. Further, it is also assumed that for a given particle size all of the particles which are within the limiting particle surface will be sampled and therefore there is no particle deposition on the external wall of the sampling probe. Thus the aspiration efficiency of the sampler is given by the expression

$$A = Q_0/Q, \quad (9)$$

where  $Q_0$  is the flux of air which is enclosed by the particle limiting surface at the upstream location AA' and  $Q$  is the sampled flux of air which enters the sampling probe.

When the orientation angle of the probe is  $180^\circ$ , only Vincent *et al.* (1986) have measured the aspiration efficiency for thin-walled samplers and they considered samplers with diameters  $D = 2$  and  $5$  cm, oncoming wind speeds  $U_0 = 1.0, 2.0$  and  $3.8 \text{ m s}^{-1}$  and sampling velocity ratios  $R = 0.67, 0.87, 1.0$  and  $2.0$ . They used two cylindrical, thin-walled, shallow-tapered samplers with a sharp edge. This geometry is slightly different from our idealized "thin-walled" cylindrical sampler with parallel walls. However, because of the shortage of experimental data we have had to use this data in order to compare with the results obtained from our numerical investigation.

## FLUID FLOW RESULTS

In order to reveal the general characteristics of the turbulent air flow in the vicinity of the orifice of the sampler, the streamline patterns are presented in Fig. 3 for  $D = 5$  cm,  $R = 1.0$  and  $U_0 = 1.0, 2.0$  and  $3.8 \text{ m s}^{-1}$ , where the stream function has been normalized by  $(D/2)^2 \pi U_0$ . It can be observed that as the magnitude of the velocity  $U_0$  increases, the air flow patterns do not change significantly. However, it is observed that the position of the streamlines near to the external wall of the sampler are affected by the velocity  $U_0$  such that the larger the value of the velocity  $U_0$  then the closer to the wall of the sampler are the streamlines. This means that the relative thickness of the boundary layer, which is defined as  $\delta/(D/2)$  where  $\delta$  is the thickness of the turbulent boundary-layer, decreases in size as the upstream velocity  $U_0$  increases in magnitude. Also the secondary flow which occurs just in the entrance region of the sampler increases in strength as the velocity  $U_0$  increases. The numerical results show that when the velocity  $U_0$  increases from  $1.0$  to  $3.8 \text{ m s}^{-1}$ , the distance from the plane of the orifice of the sampler to the stagnation point decreases from about  $x_s = D/2$  to about  $0.84 \times (D/2)$ . Therefore the increase in the velocity upstream of the sampler causes the stagnation point to be closer to the sampler.

In order to investigate the effect of the sampling velocity ratio,  $R$ , on the air flow, Fig. 4 gives the streamlines for  $D = 5$  cm,  $U_0 = 2.0 \text{ m s}^{-1}$  and  $R = 0.67, 1.0$  and  $2.0$ . As the sampling flow rate increases, the upstream radius of the limiting surface of air, which divides the flow sampled from that which is unsampled, varies from about  $1.38 \times (D/2)$  to about  $1.66 \times (D/2)$ , and the position of the stagnation point increases from about  $x_s = 0.9 \times (D/2)$  to about  $0.95 \times (D/2)$  as  $R$  decreases from  $2.0$  to  $0.67$ . This shows that as the sampling flow rate increases, the radius of the limiting air surface has been significantly increased but the position of the stagnation point is not significantly affected. It is also observed that the secondary flow in the vicinity of the edge of the sampler becomes smaller.

The effect of the diameter of the sampler on the streamlines is presented in Fig. 5 for  $U_0 = 2.0 \text{ m s}^{-1}$ ,  $R = 1.0$  and  $D = 2$  and  $5$  cm. It is observed that when  $D = 5$  cm the

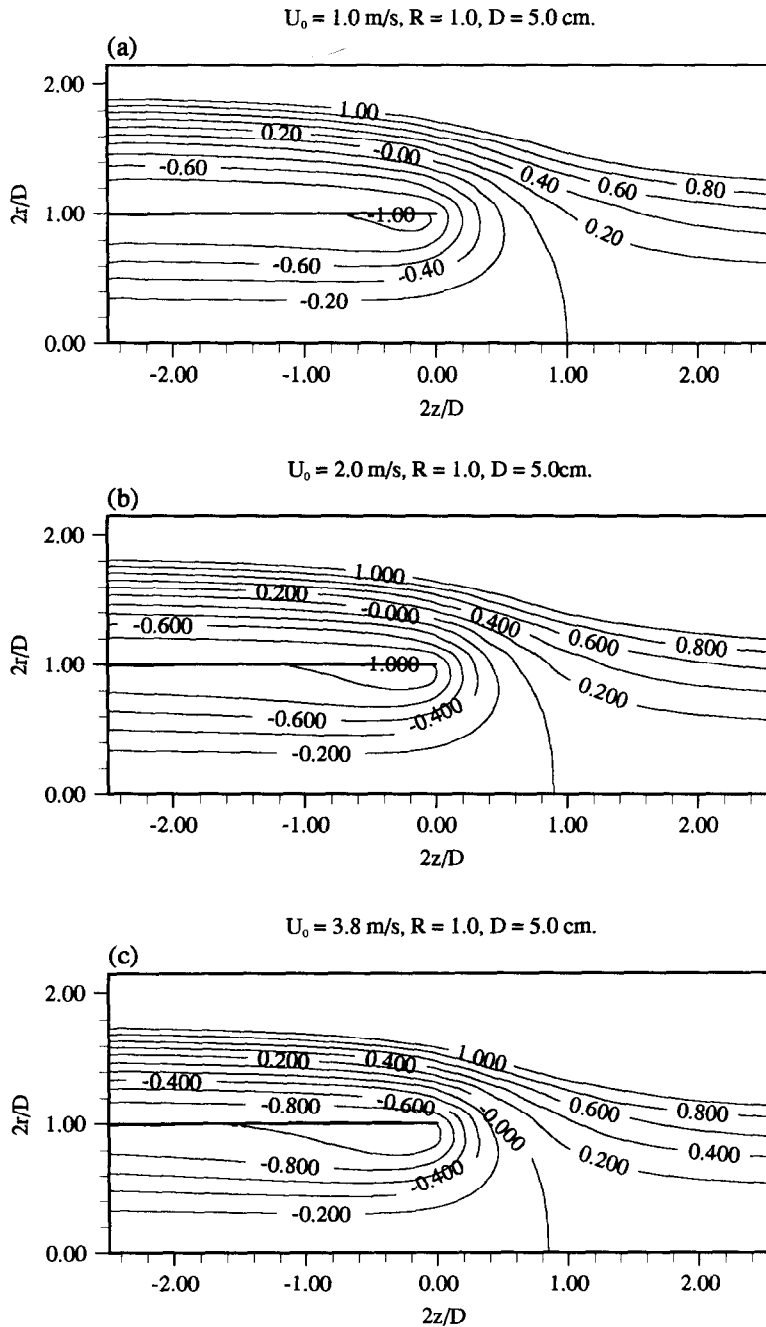


Fig. 3. The streamlines for the air flows when  $D = 5 \text{ cm}$  and  $R = 1.0$ : (a)  $U_0 = 1.0 \text{ m s}^{-1}$ ; (b)  $U_0 = 2.0 \text{ m s}^{-1}$ ; (c)  $U_0 = 3.8 \text{ m s}^{-1}$ .

streamlines near to the external wall of the sampler are closer to the wall than when  $D = 2 \text{ cm}$ . This indicates that larger samplers have a relatively smaller turbulent boundary-layer thickness. Also it is observed that the larger the diameter of the sampler, the closer to the plane of the orifice of the sampler is the stagnation point. This is because the thinner boundary-layer allows the air to flow around the edge of the sampler with a higher velocity. We also observe that the larger the value of the diameter of the sampler, the larger is the size of the secondary flow just inside the orifice of the sampler and this is because larger diameter samplers have larger velocities near to the edge of the sampler. This leads to a stronger separation, namely a larger secondary flow.

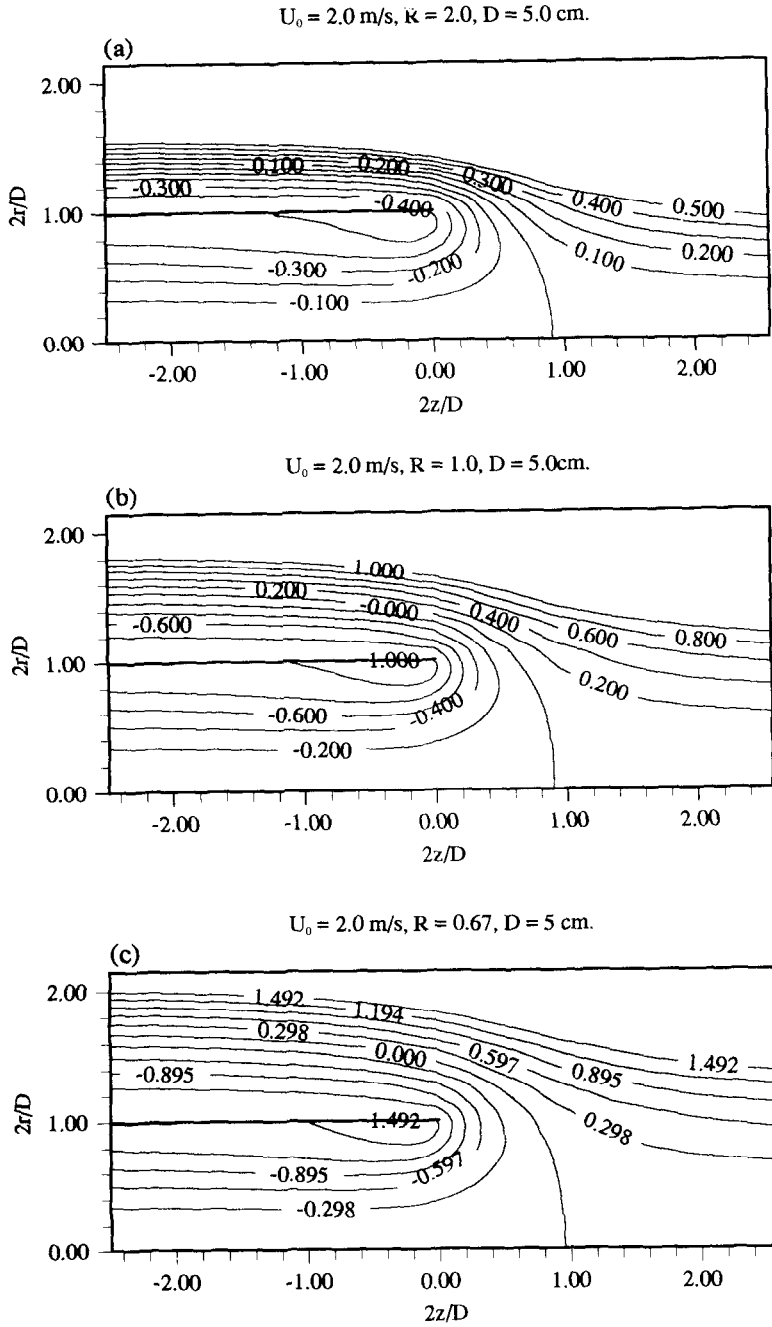


Fig. 4. The streamlines for  $U_0 = 2.0 \text{ m s}^{-1}$  and  $D = 5 \text{ cm}$ : (a)  $R = 2.0$ ; (b)  $R = 1.0$ ; (c)  $R = 0.67$ .

The velocity profile of a fully developed turbulent flow on a smooth straight wall is expressed by the logarithm formula

$$\frac{W}{U^*} = \frac{1}{\kappa} \ln \left( \text{Re} \frac{y}{D} U^* \right) + 5.5, \tag{10}$$

where  $W = w/U_0$  and  $U^* = u^*/U_0$  and  $\text{Re} = U_0 D/\nu$ . From this expression we observe that when the non-dimensional distance  $y/D$  is given then the non-dimensional velocity,  $W$ , depends on the Reynolds number  $\text{Re}$ . The larger the value of the Reynolds number the larger is the value of  $W$ . Because both increasing  $U_0$  and  $D$  produces a larger value of the

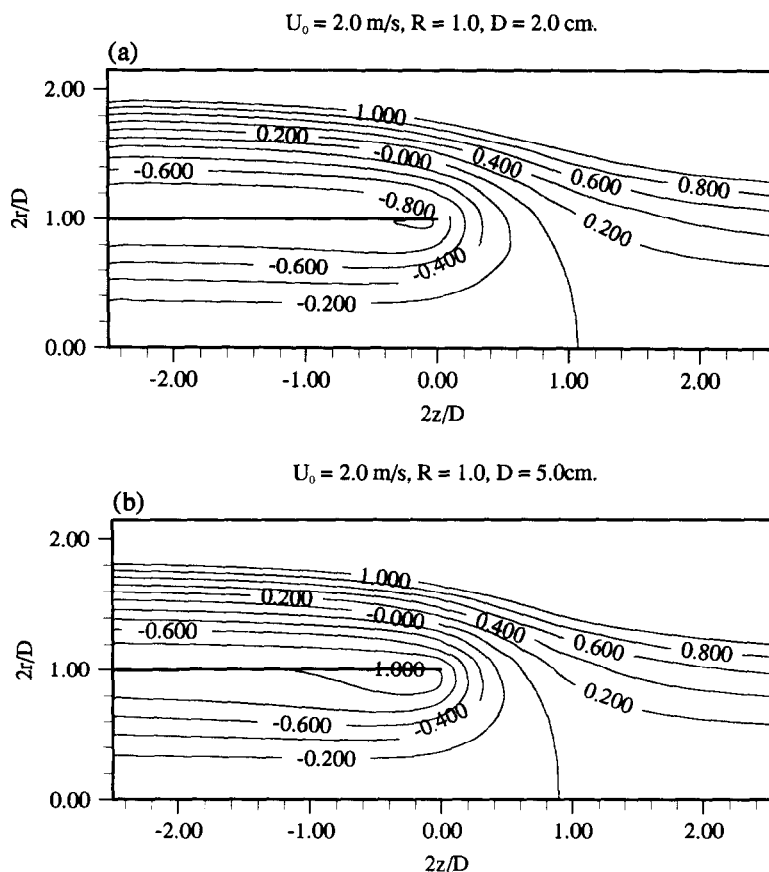


Fig. 5. The streamlines of the air flows for  $R = 1.0$  and  $U_0 = 2.0 \text{ m s}^{-1}$ : (a)  $D = 2 \text{ cm}$ ; (b)  $D = 5 \text{ cm}$ .

Reynolds number, the larger the sampler or the velocity upstream of the sampler the higher is the non-dimensional velocity within the boundary layer and the thinner is the non-dimensional boundary layer thickness. This explanation confirms what we have observed in Figs 3 and 5, namely the larger the diameter or the freestream velocity the higher is the velocity in the boundary layer and the thinner is the boundary layer thickness. It is also observed that all of the sampled air comes from the turbulent boundary layer and the larger the Reynolds number the faster is the acceleration of the air in the vicinity of the orifice of the sampler.

We therefore conclude that the effect of a relatively low value of the Reynolds number on the sampling process cannot be ignored. This means that for relatively slow freestream air speeds, or samplers of small diameter, the Reynolds number may significantly affect the sampling process.

#### ASPIRATION EFFICIENCY

As discussed above, the diameter of the sampler and the freestream velocity can significantly affect the characteristics of the turbulent boundary-layer and therefore in this paper we present the results for different fixed values of  $U_0$  in order to more clearly illustrate the effects of the Stokes number  $St$ , the diameter of sampler  $D$  and the sampling velocity ratio  $R$  on the aspiration efficiency of the sampler. Figure 6a shows the aspiration efficiency  $A$  as a function of the Stokes number,  $St$ , when  $U_0 = 3.8 \text{ m s}^{-1}$  for the two sampler diameters  $D = 2.0$  and  $5.0 \text{ cm}$ , and  $R = 0.67, 1$  and  $2$ . Comparisons have also been made with the experimental data of Vincent *et al.* (1986). All the numerical and experimental data show that the aspiration efficiency steadily decreases as the Stokes number increases and both

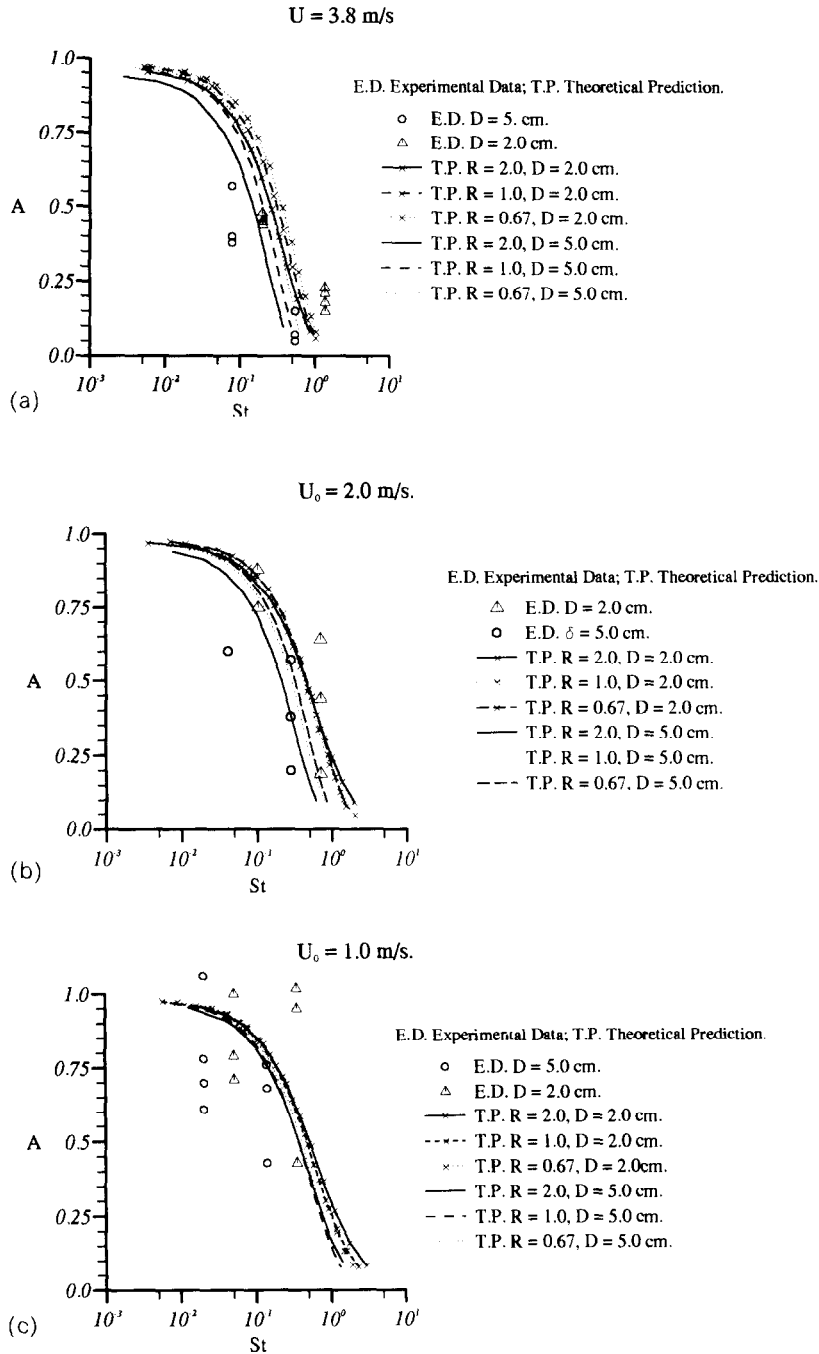


Fig. 6. The variation of the aspiration efficiency as a function of the Stokes number: (a)  $U_0 = 3.8 \text{ m s}^{-1}$ ; (b)  $U_0 = 2.0 \text{ m s}^{-1}$ ; (c)  $U_0 = 1.0 \text{ m s}^{-1}$ . The experimental data have been taken from Table 3 of Vincent *et al.* (1986).

sets of results have very similar tendencies for the two sampler diameters and for all of the sampling velocity ratios. In Fig. 6a the numerical results and experimental data show that for any sampling velocity ratio, the larger the diameter of the sampler the smaller is the aspiration efficiency. This is because the larger the sampler the higher is the velocity in the boundary layer upstream of the sampler and thus the particles in this boundary layer have a larger inertia which causes them to be sampled less easily. This phenomenon was also observed by Vincent *et al.* (1986). However, the physical reason for this behaviour was not

revealed and also in the recent work of Tsai and Vincent (1993) the diameter of the sampler as an independent parameter was not considered. It is also observed that increasing the value of the Reynolds number leads to a thinner turbulent boundary-layer which results in a smaller portion of the air which is sampled coming from the boundary layer. Therefore it can be expected that when the Reynolds number is sufficiently high the effect of the boundary layer on the aspiration efficiency will disappear. Based on both analyses of the characteristics of the air flow and the aspiration efficiency we conclude that the Reynolds number is an important independent parameter of the sampling process unless the size of the sampler is very large, or the freestream velocity is very high.

Also, from Fig. 6a we observe that as the value of  $R$  decreases, for example by increasing the sampling flow rate, the aspiration efficiency increases. As the particles approach the orifice of the sampler they accelerate due to the existence of the accelerating region in the vicinity of the edge of the orifice of the sampler. Very near to the wall of the sampler the acceleration of the air in the axial direction is much greater than that in the radial direction. Increasing the distance from the wall the acceleration in the axial direction decreases but the acceleration in the radial direction increases. As the sampling flow rate decreases, i.e. as the value of  $R$  increases, the limiting stream surface, which separates the sampled from the unsampled air, becomes closer to the external wall of the sampler. Near the wall of the sampler the particles undergo a higher acceleration in the axial direction than in the radial direction and this results in a decrease in the aspiration efficiency. As the sampling flow rate increases, i.e. as the value of  $R$  decreases, the limiting stream surface increases its distance from the external wall of the sampler. Then, even further from the wall of the sampler the particles undergo a lower acceleration in the axial direction than in the radial direction and this results in an increase in the aspiration efficiency. In the experimental work of Vincent *et al.* (1986) an effect of the sampling velocity ratio on the aspiration efficiency was not found and a possible reason for this could be the shortage of the experimental data because for each sampler and freestream velocity only one or two sets of data for each value of  $R$  were obtained.

Figure 6b shows the aspiration efficiency as a function of the Stokes number  $St$  when  $U_0 = 2.0 \text{ m s}^{-1}$ ,  $R = 0.67, 1$  and  $2$  and for the two samplers of diameters  $D = 2.0$  and  $5.0 \text{ cm}$ . It is observed that the effect of the Stokes number on the aspiration efficiency is similar to the situation when  $U_0 = 3.8 \text{ m s}^{-1}$ , see Fig. 6a. Both the numerical results and the experimental data show that the aspiration efficiency is lower for the larger value of  $D$ . It is also observed from Fig. 6b that the sampling velocity still affects the aspiration efficiency at large values of  $D$  but this effect is smaller at the smaller values of  $D$ . The comparison between the theory and experiment for the aspiration efficiency is good.

Figure 6c shows the aspiration efficiency as a function of the Stokes number,  $St$ , when  $U_0 = 1.0 \text{ m s}^{-1}$ ,  $R = 0.67, 1$  and  $2$  and for the two sampler diameters  $D = 2.0$  and  $5.0 \text{ cm}$ . Once again the numerical results show that the Stokes number is a very important parameter which dominates the sampling process. In this case, in which there is a low freestream velocity, the numerical results still predict a decreasing value of the aspiration efficiency as the diameter of the sampler increases, albeit at a slower rate. Also the results show that the aspiration efficiency is not significantly affected by the sampling velocity ratio for both of the diameters of the sampler considered. This indicates that the effects of the sampling velocity ratio on the aspiration efficiency increases with increasing freestream velocity.

When the freestream velocity  $U_0 = 2.0$  and  $3.8 \text{ m s}^{-1}$ , the experimental data in Figs 6a and 6b show less scatter than they do in Fig. 6c when  $U_0 = 1.0 \text{ m s}^{-1}$  for the aspiration efficiency as a function of the Stokes number. Although there is much scatter in the experimental data when  $U_0 = 1.0 \text{ m s}^{-1}$  the theoretically predicted curves in Fig. 6c reasonably represent the tendency of the aspiration efficiency as a function of the Stokes number. A possible explanation for this could be that at the larger freestream velocities, i.e. at larger values of the Reynolds number, the turbulent eddies are of a small scale and the fluctuating velocities are of high frequency and also the larger freestream velocities lead to a larger particle Stokes number of particle. At the smaller values of the Reynolds number

the turbulent eddies are of a larger scale and the fluctuating velocities are of low frequency and the particles which have a smaller Stokes number due to smaller freestream velocity, respond faster to the fluctuating fluid velocity. Therefore we postulate that the large-scale turbulent eddies, the low frequency fluctuating velocities and the small Stokes number produce the scatter in the experimental data.

## CONCLUSIONS

The sampling mechanism of an idealized thin-walled cylindrical sampler at an angle of inclination of  $180^\circ$  has been investigated by employing numerical techniques and the turbulent  $k-\epsilon$  model. Good agreement between the numerical predictions and the available experimental data has been obtained and we conclude that:

(a) When a thin-walled cylindrical sampler is facing directly backwards to the oncoming wind, the inertia of the particles, namely the particle Stokes number,  $St$ , dominates the sampling process for any size of sampler, freestream velocity and sampling velocity ratio.

(b) The turbulent-boundary flow along the external wall of the sampler is of secondary importance in calculating the aspiration efficiency. The increase in the diameter of the sampler, or the magnitude of the freestream speed leads to a decrease in the relative thickness of the turbulent boundary-layer and this produces a decrease in the aspiration efficiency.

(c) When the freestream velocity is fixed, the sampling velocity ratio has a smaller effect on the aspiration efficiency than does the diameter of the sampler. The effect of the sampling velocity ratio becomes significant only for large values of the sampler diameter  $D$  or freestream velocity  $U_0$ .

Future research work should include an investigation into the influence of the bluntness of the sampler, in particular the impaction of the particles on the leading face of the sampler, the effect of particle diffusion on the aspiration efficiency and calm air sampling through thin-walled tubes.

*Acknowledgement*—The financial support of the Health and Safety Executive and SERC is gratefully acknowledged.

## REFERENCES

- Badzioch, S. (1959) Collection of gas-borne dust particles by means of an aspirated sampling nozzle. *Br. J. appl. Phys.* **10**, 26–32.
- Belyaev, S. P. and Levin, L. M. (1974) Techniques for collection of representative aerosol samplers. *J. Aerosol Sci.* **5**, 325–338.
- Davies, C. N. and Subari, M. (1982) Aspiration above wind velocity of aerosols with thin-walled nozzles facing and at right angles to the wind direction. *J. Aerosol Sci.* **13**, 59–71.
- Dunnett, S. J. (1990) Mathematical modelling of aerosol sampling with thin-walled probes at yaw orientation with respect to the wind. *J. Aerosol Sci.* **21**, 947–956.
- Durham, M. D. and Lundgren, D. A. (1980) Evaluation of aerosol aspiration efficiency as a function of Stokes' number, velocity ratio and nozzle angle. *J. Aerosol Sci.* **11**, 179–188.
- Grinshpun, S., Willeke, K. and Kalatoor, S. (1993) A general equation for aerosol aspiration by thin-walled sampling probes in calm and moving air. *Atmos. Envir.* **27A**, 1459–1470.
- Hangal, S. and Willeke, K. (1990) Aspiration efficiency: unified model for all forward sampling angles. *Envir. Sci. Technol.* **24**, 688–691.
- Ingham, D. B. and Wen, X. (1993) Disklike body sampling in a turbulent wind. *J. Aerosol Sci.* **24**, 629–642.
- Jayasekera, P. N. and Davies, C. N. (1980) Aspiration below wind velocity of aerosols with sharp-edged nozzles facing the wind. *J. Aerosol Sci.* **11**, 535–547.
- Lauder, B. E. and Spalding, D. B. (1974) The numerical computation of turbulent flows. *Comput. Methods appl. mech. Engrg* **3**, 269–289.
- Okazaki, K., Wiener, R. W. and Eilleke, K. (1987) Nonisoaxial aerosol sampling mechanisms controlling the overall sampling efficiency. *Envir. Sci. Technol.* **21**, 183–187.
- Patankar, S. V. (1980) *Numerical Heat Transfer and Fluid Flow*. Hemisphere, New York.
- Peskin, R. L. (1962) The diffusivity of small suspended particles in turbulent fluids. The National AIChE, Meeting, Baltimore.
- Ruping, G. (1968) *Staub-Reinlalt. Luft* **28**, 1 (English translation).
- Sehmel, G. A. (1967) Velocity of air samplers as affected by anisokinetic sampling and deposition within sampling line. *Proc. of the Symposium on Assessment of Airborne Radioactivity*, Vienna, pp. 727–735.

- Shuen, J.-S., Chen, L.-D. and Fearh, G. M. (1983) Evaluation of a stochastic model of particle dispersion in a turbulent round jet. *A.I.Ch.E. J.* **29**, 167–170.
- Tsai, P.-J. and Vincent, J. H. (1993) Impaction model for the aspiration efficiencies of aerosol samplers at large angles with respect to the wind. *J. Aerosol Sci.* **24**, 919–928.
- Van Doormaal, J. P. and Raithby, G. D. (1984) Enhancements of the SIMPLE method for predicting incompressible fluid flows. *Numer. Heat Transfer* **7**, 147–163.
- Vincent, J. H., Stevens, D. C., Mark, D., Marshall, M. and Smith, T. A. (1986) On the aspiration characteristics of large-diameter, thin-walled aerosol sampling probes at yaw orientations with respect to the wind. *J. Aerosol Sci.* **17**, 211–224.
- Vitols, V. (1966) Theoretical limits of errors due to anisokinetic sampling of particulate matter. *J. Air Pollut. Control Assoc.* **16**, 79–84.
- Wen, X. and Ingham, D. B. (1993) A new method for accelerating the rate of convergence of the SIMPLE-like algorithm. *Int. J. Numer. Methods Fluids* **7**, 385–400.